3D MAS NMR Experiment Utilizing Through-Space

Citation: Donovan, Kevin J. et al. "3D MAS NMR Experiment Utilizing Through-Space 15N–15N Correlations." Journal of the American Chemical Society 139, 19 (May 2017): 6518–6521 © 2017 American Chemical Society

As Published: http://dx.doi.org/10.1021/jacs.7b01159

Publisher: American Chemical Society (ACS)

Persistent URL: http://hdl.handle.net/1721.1/114858

Version: Author's final manuscript: final author's manuscript post peer review, without publisher's formatting or copy editing

A 3D MAS NMR experiment utilizing through-space ^{15}N-^{15}N correlations

Kevin J. Donovan[†‡], Robert Silvers[†‡], Sara Linse[§], and Robert G. Griffin[†*]

†Department of Chemistry and Francis Bitter Magnet Laboratory, Massachusetts Institute of Technology, Cambridge, Massachusetts 02139

§ Department of Biochemistry and Structural Biology, Lund University, Lund, Sweden

‡These authors contributed equally

Supporting Information Placeholder

ABSTRACT: We demonstrate a novel 3D NNC magic angle spinning (MAS) NMR experiment that generates ^{15}N-^{15}N internuclear contacts in protein systems using an optimized ^{15}N-^{15}N proton assisted recoupling (PAR) mixing period and a ^{13}C dimension for improved resolution. The optimized PAR condition permits the acquisition of high signal-to-noise 3D data that enables backbone chemical shift assignments using a strategy that is complementary to current schemes. The spectra can also provide distance constraints. The utility of the experiment is demonstrated on an $M_0A\beta_{1\text{-}42}$ fibril sample that yields high-quality data that is readily assigned and interpreted. The 3D NNC experiment therefore provides a powerful platform for solid-state protein studies and is broadly applicable to a variety of systems and experimental conditions.

Protein structure determination using magic angle spinning (MAS) NMR spectroscopy invariably begins with chemical shift assignments, where each distinct resonance is associated with a specific nuclear site. Resonance assignment is typically accomplished using 2D and 3D experiments where magnetization is transferred among ^{1}H/^{13}C/^{15}N nuclei using dipole recoupling experiments designed to reintroduce the coupling attenuated by MAS. While this initial step is of crucial importance, it is often tedious and challenging. Homonuclear dipolar recoupling in 2D and 3D assignment experiments predominantly utilizes ^{13}C-^{13}C magnetization transfer, due to the prevalence of ^{13}C nuclei in biological samples, and to a favorable gyromagnetic ratio of ^{13}C. In principle, it is also possible to use ^{15}N-^{15}N couplings for assignments and structural studies, an approach that is appealing because of the excellent resolution of the ^{15}N dimension. Accordingly, previous approaches employed proton driven spin diffusion (PDSD) techniques to generate ^{15}N-^{15}N correlation spectra of three model peptides[1-2], three model proteins[3-5], and more recently, oriented membranes[6]. Additionally, a ^{15}N-^{15}N spectrum obtained using an early version of proton assisted recoupling (PAR) was reported[7]. Despite the fact that these initial results are very promising, ^{15}N-^{15}N techniques have not evolved to be part of the standard repertoire of MAS protein experiments, primarily for three reasons: (1) the sensitivity in the PDSD and the initial PAR spectra is low and does not permit extension to higher dimensions; (2) cross peaks for long-rang contacts are often missing from the spectra; and (3) the mixing times are 2-5 s and therefore the total experimental time is long. Here we describe a novel 3D NNC experiment (depicted in **Figure 1A**) that utilizes an *optimized* ^{15}N-^{15}N PAR protocol that yields excellent ^{15}N sensitivity, and therefore easily extends to a third directly detected ^{13}C dimension to further increase the resolution. Furthermore, the PAR mixing sequence is short (20 ms) and the spectra display an abundance of cross peaks.

As mentioned above, 3D MAS experiments usually utilize ^{13}C-^{13}C correlations (generated using RFDR[8-9], DARR[10], PDSD[11-12], or PAR[13] mixing, amongst others) that are resolved with a ^{15}N dimension. The transfer from ^{15}N to ^{13}C is typically based on SPECIFIC-CP[14-16] or

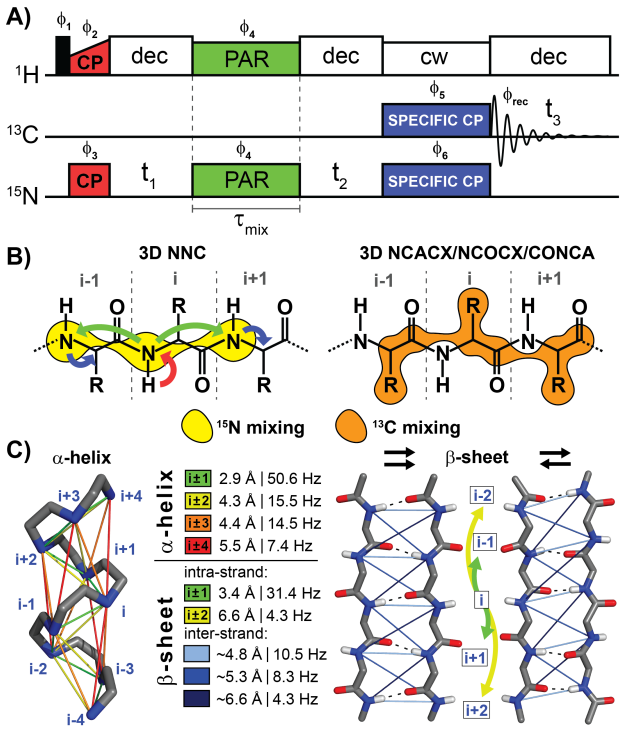

Figure 1: The 3D NNC pulse sequence is shown in A) with phase cycling: ϕ_1 = 02, ϕ_2 = 0022, ϕ_3 = 1, ϕ_4 = 2002, ϕ_5 = 0123, ϕ_6 = 2002 0220, ϕ_{rec} = 0123 2301. The CP, PAR, and SPECIFIC-CP blocks are color coded to arrows in (B) illustrating the corresponding magnetization transfer. Additionally, B) contrasts the mode of mixing for the NNC experiment, and commonly used protocols (NCACX, NCOCX, CONCA), illustrating their complementary information due to reliance on separate contacts. C) visualizes the internuclear distances and corresponding dipole coupling values for a range of ^{15}N-^{15}N contacts in α-helices and parallel and anti-parallel β-sheets. The residue interval label (i.e. i ± 1, i ± 2, etc.) is color coded to the lines/arrows illustrating transfer. The ^{15}N-^{15}N

other ^{15}N-^{13}C transfer techniques[17-19]. This combination leads to a suite of experiments used for backbone resonance assignments that includes a combination of NCA/NCACX/NCACB[20-25], NCO/NCOCX[21-25], and CONCA/CANCO[23-25]. The 3D NNC, however, allows for the acquisition of non-redundant and complementary information that is otherwise inaccessible and thus facilitates comprehensive assignment strategies when combined with other data sets. This unique sequence shares features with previous ^{15}N-^{15}N correlation experiments in liquids[26-27] as well as solid, deuterated samples at high MAS frequencies[28]. Additionally, direct ^{15}N detection has recently been used for proteins in solution experiments[29]. However, the NNC is distinguished from the above experiments since it utilizes through-space ^{15}N-^{15}N dipole cou-

pling to mediate coherence transfer and generate homonuclear contacts. However, ^{15}N homonuclear dipolar recoupling remains difficult to implement in non-model samples such as M$_0$Aβ_{1-42} (as opposed to N-*f*-MLF-OH[30] or GB1[31]), the 42 amino acid protein that forms toxic fibril species associated with Alzheimer's disease[32-46]. While this system is well suited for solid state NMR analysis because of its monodispersity and small molecular size (enabling high sensitivity), it presents many difficulties for collecting high-quality data as it is significantly more structurally heterogeneous, and less static than any of the usual model systems. It is for this reason that we have chosen M$_0$Aβ_{1-42} to test the efficiency of the NNC protocol.

To demonstrate the importance of PAR mixing we compared the signal-to-noise ratio, the number of observed cross peaks, and maximum distance observed for three available ^{15}N-^{15}N homonuclear mixing schemes: RFDR (τ_{mix} = 12.8 ms), PDSD (τ_{mix} = 4 s), and PAR (τ_{mix} = 20 ms). These results are illustrated in **Figure 2**. We found that ^{15}N-^{15}N mixing with the first-order recouping sequence RFDR[8-9] (**Figure 2A**), yields no cross-peaks due to the small homonuclear dipolar couplings <50 Hz (**Figure 1C**). Using ^{15}N-^{15}N PDSD[11-12], a second-order recoupling sequence, we observed a limited number of cross peaks (**Figure 2B**). However, in addition to the minimal quantity of cross-peaks, this experiment requires τ_{mix} = 4 s, and all the cross-peaks are assigned to distances <3.5 Å (i±1). In contrast, the ^{15}N-^{15}N PAR experiment, also a second-order recoupling sequence, shows significantly more cross-peaks than the PDSD, and distances of up to 6.8 Å are observed. These are apparent in **Figure 2C. Figure 2D** compares 1D traces from the RFDR, PDSD, and PAR spectra, clearly showing the superior signal intensity given by PAR, and the presence of additional

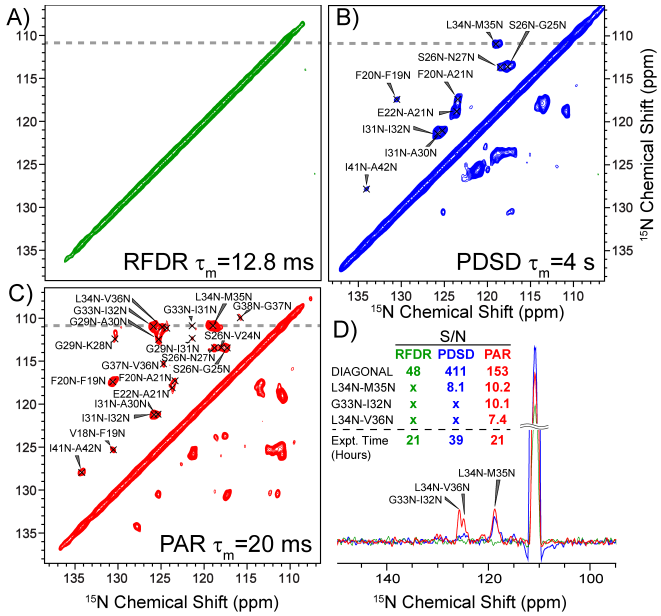

Figure 2: 2D ^{15}N-^{15}N homonuclear correlation spectra on M$_0$Aβ_{1-42}. A) gives a comparison of 1D traces extracted from the 2D spectra in B)-D) as indicated by a gray line, with a comparison of measured signal-to-noise (S/N) and total experiment times. Panels B)-D) show a τ_{mix} = 12.8 ms ^{15}N-^{15}N RFDR (green), a τ_{mix} = 20 ms ^{15}N-^{15}N PAR (red), and a τ_{mix} = 4 s ^{15}N-^{15}N PDSD (blue), respectively. Cross-peak assignments are shown.

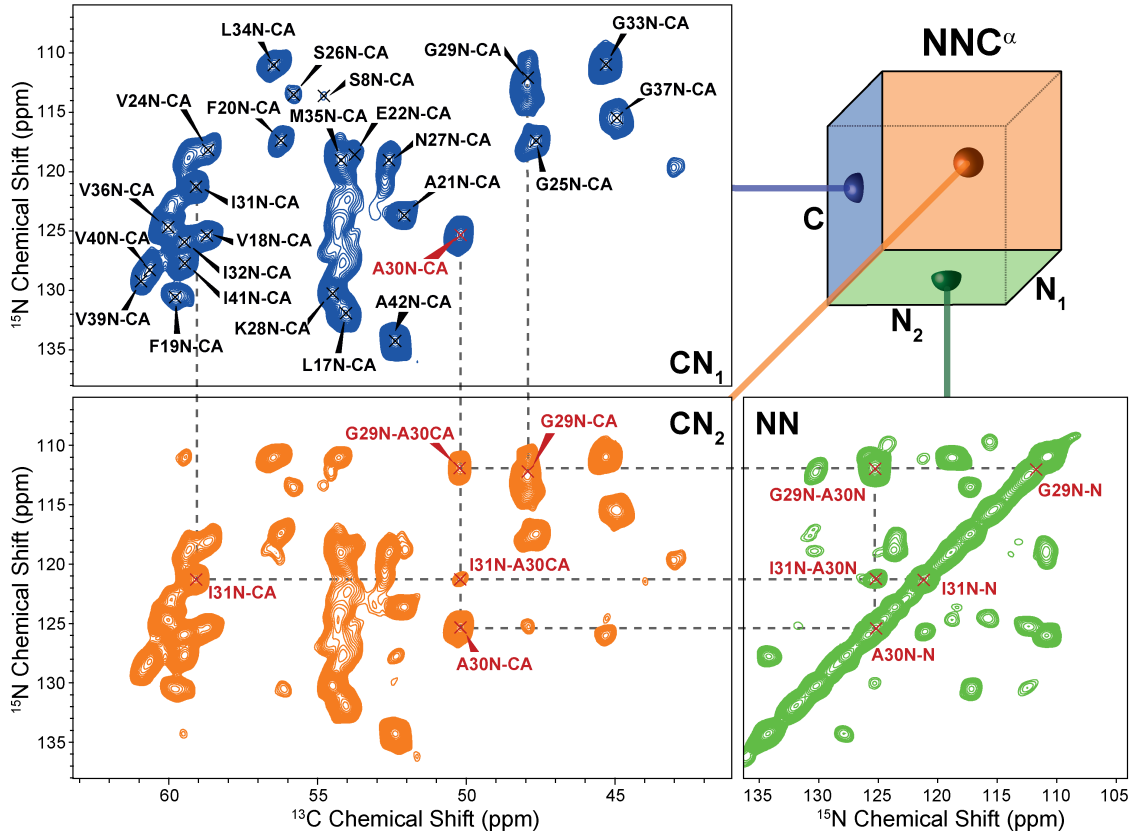

Figure 3: 3D NNC$^{\alpha}$ projections of M$_0$Aβ_{1-42}. One CN projection (CN$_1$) shows one peak per residue correlating the nitrogen and the C$^{\alpha}$ of the same amino acid i. The second CN projection (CN$_2$) is identical to CN$_1$ plus additional peaks due to NN-mixing. For each C$^{\alpha}$/N pair (which forms the diagonal peak) there are peaks that correspond to nearby ^{15}N sites, most prominently the i±1 backbone amide ^{15}N nuclei. The third projection (NN) is identical to a 2D ^{15}N-^{15}N PAR spectrum showing the backbone nitrogen of residue i as diagonal and other peaks (mostly backbone nitrogen of residues i±1) as cross-peaks. The 3D spectrum was recorded on a Bruker Avance III 800 MHz spectrometer at $\omega_r/2\pi$ = 20 kHz with temperature set to 277 K. A more detailed assignment is shown in Figure S1.

cross peaks that are attributed to long-range contacts (which are not present in either the RFDR or PDSD spectra). It is also important to note that the total acquisition time for the 2D PAR in **Figure** was around 21 h, while the PDSD required 39 h, nearly twice as long.

The 2D ^{15}N-^{15}N spectra utilize an optimum PAR matching condition, enabling this innovative approach to backbone resonance assignments on disease-relevant $M_0A\beta_{1-42}$. The optimum condition was obtained using a high-throughput protocol to evaluate magnetization transfer across an array of conditions, as described in detail in the Supporting Information. While the PAR mixing period in the NNC experiment generates ^{15}N-^{15}N contacts that are both short-range (between neighboring residues) and long-range (between non-neighboring residues), only the short-range contacts are useful for sequential assignment. Thus, the PAR mixing time can be adjusted to maximize short-range over long-range contacts. Long-range contacts

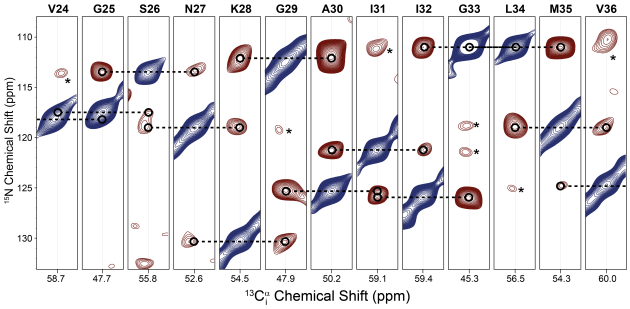

Figure 2: Strip plot of the 3D NNC$^{\alpha}$ of $M_0A\beta_{1-42}$. Each strip displays the diagonal peak of residue i (blue) and several cross-peaks (red). The most prominent cross-peaks at 20 ms PAR mixing are from residues i±1, although cross-peaks from residues i±2 can be present (*). The sequential backbone walk is indicated by dashed lines. Colors do not indicate sign and are solely used as visual aids.

are undesirable for sequential assignment purposes as they may augment spectral congestion and/or obfuscate the assignment process. However, long-range contacts are essential for structural characterization, and can be extracted from NNC spectra collected at longer mixing times. The NNC spectra shown here were collected with a PAR τ_{mix}=20 ms, which yields predominantly short-range contacts in $M_0A\beta_{1-42}$, with only minor long-range contacts that are easily distinguished by significantly weaker intensities.

The NNC pulse sequence (as shown in **Figure 1A**) consists of three transfer steps: ^{1}H-^{15}N CP, ^{15}N-^{15}N PAR mixing, and ^{15}N-^{13}C SPECIFIC-CP, where the magnetization is selectively transferred to either the Cα or the CO nuclei to generate either an NNC$^{\alpha}$ (see **Figures 2 and 3**) or an NNC^{O} (see **Figures S2 and S3**) spectrum. Transfer efficiencies for the ^{15}N-^{15}N PAR mixing alone (i.e. in comparison to ^{1}H-^{15}N CP and ^{15}N-^{13}C SPECIFIC-CP without ^{15}N-^{15}N PAR mixing) are shown in **Figure S4** for N-*f*-MLF-OH and $M_0A\beta_{1-42}$. The remaining ^{15}N magnetization after ^{15}N-^{15}N PAR mixing depends on the mixing time and relaxation rates. After 20 ms of PAR mixing, 53% and 20% of the magnetization remain for N-*f*-MLF-OH and $M_0A\beta_{1-42}$, respectively. Besides the ^{15}N-^{15}N PAR mixing, the total efficiency of the 3D NNC experiment depends on the heteronuclear transfer, which is coupled to the selectivity and also the sample and the experimental conditions chosen (vide infra).

A comparison of NNC$^{\alpha}$ and NNC^{O} for $M_0A\beta_{1-42}$ shows the NNC$^{\alpha}$ spectrum to have superior resolution due to larger chemical shift dispersion in the C$^{\alpha}$ spectral region than the CO spectral region. However, the diagonal of the NNC^{O} spectrum contains additional information as it displays correlations between the ^{15}N of residue *i* and the ^{13}CO of residue *i-1*, whereas the diagonal of the NNC$^{\alpha}$ shows correlations only between nuclei within the same residue. **Figure 1B** illustrates the internuclear correlations obtained in an NNC experiment vs. commonly used ^{13}C-^{13}C based experiments, and **Figure 1C** shows internuclear distances (and corresponding dipole coupling values) in standard α-helix as well as parallel and anti-parallel β-sheet structures for the ^{15}N-^{15}N contacts observed with the 3D NNC sequence.

A distinct advantage of the NNC experiment is the increased resolution gained from the inclusion of a 3rd (^{13}C) dimension. The 2D ^{15}N-^{15}N PAR spectrum shown in **Figure** displays efficient magnetization transfer, but limited resolution. However, both the 3D NNC$^{\alpha}$ as well as the 3D NNC^{O} spectra have immensely improved resolution over their 2D counterparts.

Figure 3 displays 2D projections for each of the three unique faces of the NNC cube. The CN_1 projection is virtually identical to an NCA experiment[22] or the C$^{\alpha}$ region of a short-mixing ZF-TEDOR experiment[47]. Hence, CN_1 shows one peak per residue correlating the nitrogen and the C$^{\alpha}$ of the same amino acid. The CN_2 projection is identical to CN_1 plus additional peaks due to ^{15}N-^{15}N mixing. For each C$^{\alpha}$/N pair (which forms the diagonal peak) there are peaks that correspond to nearby ^{15}N sites, most prominently the *i±1* backbone amide ^{15}N nuclei. The third projection (NN) is identical to a 2D ^{15}N-^{15}N PAR spectrum showing the backbone nitrogen of residue i as a diagonal peak, as well as other coherences (mostly backbone nitrogen of residues *i±1*) as cross-peaks. The correlations between these three projections and the information therein is shown as example for residue A30 of $M_0A\beta_{1-42}$ in **Figure** and in greater detail in **Figure S1**.

For resonance assignment, each diagonal peak can be arranged in a strip plot (**Figure 4**) that displays the sequential walk. Each strip shows the diagonal peak (blue) and one or more cross-peaks (red), unless overlapping with other peaks. Typically, the strongest cross-peaks are of i±1 residues. Occasionally, *i*±2 residues can be present (as discussed earlier), for example between N27 and G29 (6.6 Å, D_{NN}=4.3 Hz), I31 and G33 (6.8 Å, D_{NN}=3.93 Hz), as well as G33 and M35 (5.8 Å, D_{NN}=6.3 Hz).

In summary, the 3D NNC experiment presented here provides a novel and compelling approach to protein backbone assignments by generating unique data not otherwise accessible. Typically, ^{13}C-^{13}C mixing schemes are used to correlate consecutive residues in proteins while using ^{15}N to resolve spectral crowding. The 3D NNC experiment, however, generates ^{15}N-^{15}N correlations and uses ^{13}C for spectral decongestion. Application of the PAR mixing scheme coupled with a careful optimization of the PAR fields provides efficient ^{15}N homonuclear magnetization transfer, enabling high signal-to-noise data in 3D settings. While this initial demonstration serves as a showcase of the NNC experimental protocol, variations are readily envisaged with different heteronuclear transfer techniques to accomplish the ^{15}N-^{13}C transfer including adiabatic passage[48], Lee-Goldburg decoupling[49], TEDOR[18], PAIN-CP[19], and RESPIRATION-CP[17], amongst others. These may offer improved selectivity and/or efficiency depending on the sample and the experimental conditions (i.e. spinning frequency and magnetic field). Furthermore, the NNC sequence naturally lends itself to other experiments of higher dimensionality that include additional transfer steps (e.g. a 4D NNCC sequence) and ^{1}H detection. As experimental NMR transitions to higher magnetic fields and faster sample spinning, we expect the NNC protocol to have a continued relevance as PAR has previously shown excellent functionality at higher spinning frequencies (i.e. 65 kHz)[50]. Finally, while the NNC experiment was developed for sequential assignments, we anticipate that it will provide long-range ^{15}N-^{15}N contacts (using longer mixing times) that are highly valuable for structural characterization. We foresee this approach to be broadly applicable to a large variety of samples includ-

ing protein crystals and fibrils, nucleic acids, as well as membrane proteins and sedimented proteins.

ASSOCIATED CONTENT

Supporting Information

The Supporting Information is available free of charge on the ACS Publications website. The Supporting Information contains a detailed Experimental Section and Supporting Figures S0-S4.[8-9, 11-15, 38, 42, 51-53]

AUTHOR INFORMATION

Corresponding Author

*rgg@mit.edu

Author Contributions

‡K.J.D. and R.S. contributed equally to this work.

Notes

The authors declare no competing financial interests.

ACKNOWLEDGMENT

The research was supported by grants from the National Institutes of Biomedical Imaging and Bioengineering (EB- 001960, EB-002026, and EB-002804) to R.G.G. and by the Swedish Research Council (VR) and a European Research Council (ERC) Advanced Grant to S.L. R.S. is funded by a DFG research fellowship (SI2105/1-1).

REFERENCES

(1) Reif, B.; Hohwy, M.; Jaroniec, C. P.; Rienstra, C. M.; Griffin, R. G., *J. Magn.Res.* **2000,** *145*, 132-141.
(2) Traaseth, N. J.; Gopinath, T.; Veglia, G., *J. Phys. Chem. B* **2010,** *114*, 13872-13880.
(3) van Rossum, B.-J.; Castellani, F.; Pauli, J.; Rehbein, K.; Hollander, J.; de Groot, H. J. M.; Oschkinat, H., *J. Biomol NMR* **2003,** *25*, 217-223.
(4) Seidel, K.; Etzkorn, M.; Heise, H.; Becker, S.; Baldus, M., *ChemBioChem* **2005,** *6*, 1638-1647.
(5) Franks, W. T.; Wylie, B. J.; Stellfox, S. A.; Rienstra, C. M., *J. Am. Chem. Soc.* **2006,** *128*, 3154-3155.
(6) Mote, K. R.; Gopinath, T.; Traaseth, N. J.; Kitchen, J.; Gor'kov, P. L.; Brey, W. W.; Veglia, G., *J. Biomol. NMR* **2011,** *51*, 339.
(7) Lewandowski, J. R.; Paëpe, G. D.; Eddy, M. T.; Griffin, R. G., *J. Am. Chem. Soc.* **2009,** *131*, 5769-5776.
(8) Bennett, A. E.; Griffin, R. G.; Ok, J. H.; Vega, S., *J. Chem. Phys.* **1992,** *96*, 8624-8627.
(9) Bennett, A. E.; Rienstra, C. M.; Griffiths, J. M.; Zhen, W. G.; Lansbury, P. T.; Griffin, R. G., *J. Chem. Phys.* **1998,** *108*, 9463-9479.
(10) Takegoshi, K.; Nakamura, S.; Terao, T., *Chem. Phys. Lett.* **2001,** *344*, 631-637.
(11) Suter, D.; Ernst, R. R., *Phys. Rev. B* **1982,** *25*, 6038-6041.
(12) Szevernyi, N.; Sullivan, M.; Maciel, G., *J. Magn. Reson.* **1982,** *47*, 462-475.
(13) DePaëpe, G.; Lewandowski, J. R.; Loquet, A.; Böckmann, A.; Griffin, R. G., *J. Chem. Phys.* **2008,** *129*, 245101.
(14) Baldus, M.; Petkova, A. T.; Herzfeld, J.; Griffin, R. G., *Mol Phys* **1998,** *95*, 1197-1207.
(15) Petkova, A. T.; Baldus, M.; Belenky, M.; Hong, M.; Griffin, R. G.; Herzfeld, J., *J. Magn Reson.* **2003,** *160*, 1-12.
(16) Rienstra, C. M.; Hohwy, M.; Hong, M.; Griffin, R. G., *J. Am. Chem. Soc.* **2000,** *122*, 10979-10990.
(17) Jain, S.; Bjerring, M.; Nielsen, N. C., *J. Phys. Chem, Lett.* **2012,** *3*, 703-708.
(18) Jaroniec, C. P.; Filip, C.; Griffin, R. G., *J. Am. Chem. Soc.* **2002,** *124*, 10728-10742.
(19) Lewandowski, J. R.; De Paëpe, G.; Griffin, R. G., *J. Am. Chem. Soc.* **2007,** *129*, 728-729.
(20) Igumenova, T. I.; McDermott, A. E.; Zilm, K. W.; Martin, R. W.; Paulson, E. K.; Wand, A. J., *J. Am. Chem, Soc.* **2004,** *126*, 6720-6727.
(21) Marulanda, D.; Tasayco, M.; McDermott, A.; Cataldi, M.; Arriaran, V.; Polenova, T., *J. Am. Chem. Soc.* **2004,** *126*, 16608-16620.
(22) Pauli, J.; Baldus, M.; Rossum, B. v.; de Groot, H.; Oschkinat, H., *ChemBioChem* **2001,** *2*, 272-281.
(23) Shi, L.; Lake, E.; Ahmed, M.; Brown, L.; Ladizhansky, V., *BBA - Biomembranes* **2009,** *1788*, 2563-2574.
(24) Sperling, L. J.; Nieuwkoop, A. J.; Lipton, A. S.; Berthold, D. A.; Rienstra, C. M., *J. Biomol. NMR* **2010,** *46*, 149-155.
(25) Schuetz, A.; Wasmer, C.; Habenstein, B.; Verel, R.; Greenwald, J.; Riek, R.; Böckmann, A.; Meier, B. H., *ChemBioChem* **2010,** *11*, 1543-1551.
(26) Frenkiel, T.; Bauer, C.; Carr, M. D.; Birdsall, B.; Feeney, J., *J. Magn. Reson* **1990,** *90*, 420-425.
(27) Diercks, T.; Coles, M.; Kessler, H., *J. Biomolecular NMR* **1999,** *15*, 177-180.
(28) Andreas, L. B.; Stanek, J.; Le Marchand, T.; Bertarello, A.; Paepe, D. C.-D.; Lalli, D.; Krejčíková, M.; Doyen, C.; Öster, C.; Knott, B.; Wegner, S.; Engelke, F.; Felli, I. C.; Pierattelli, R.; Dixon, N. E.; Emsley, L.; Herrmann, T.; Pintacuda, G., *J. Biomol. NMR* **2015,** *62*, 253-261.
(29) Takeuchi, K.; Arthanari, H.; Shimada, I.; Wagner, G., *J. Biomol. NMR* **2015,** *63*, 323-331.
(30) Rienstra, C. M.; Tucker-Kellogg, L.; Jaroniec, C. P.; Hohwy, M.; Reif, B.; McMahon, M. T.; Tidor, B.; Lozano-Pérez, T.; Griffin, R. G., *Proc. Nat'l Acad. Sci.* **2002,** *99*, 10260-10265.
(31) Frericks Schmidt, H. L.; Sperling, L. J.; Gao, Y. G.; Wylie, B. J.; Boettcher, J. M.; Wilson, S. R.; Rienstra, C. M., *J Phys. Chem. B* **2007,** *111*, 14362-14369.
(32) Sachse, C.; Fändrich, M.; Grigorieff, N., *Proc. Nat'l Acad. Sci* **2008,** *105*, 7462-7466.
(33) Ahmed, M.; Davis, J.; Aucoin, D.; Sato, T.; Ahuja, S.; Aimoto, S.; Elliott, J. I.; Van Nostrand, W. E.; Smith, S. O., *Nature Struc. Mole. Bio***2010,** *17*, 561-567.
(34) Bertini, I.; Gonnelli, L.; Luchinat, C.; Mao, J.; Nesi, A., *J. Am. Chem. Soc.* **2011,** *133*, 16013-16022.
(35) Fändrich, M.; Schmidt, M.; Grigorieff, N., *Trends in Biochem. Sci.* **2011,** *36*, 338-345.
(36) Lopez del Amo, J.-M.; Schneider, D.; Loquet, A.; Lange, A.; Reif, B., *J. Biomol. NMR* **2013,** *56*, 359-363.
(37) Lu, J.-X.; Qiang, W.; Yau, W.-M.; Schwieters, Charles D.; Meredith, Stephen C.; Tycko, R., *Cell* **2013,** *154*, 1257-1268.
(38) Colvin, M. T.; Silvers, R.; Frohm, B.; Su, Y.; Linse, S.; Griffin, R. G., *J. Am. Chem. Soc.* **2015,** *137*, 7509-7518.
(39) Schmidt, M.; Rohou, A.; Lasker, K.; Yadav, J. K.; Schiene-Fischer, C.; Fändrich, M.; Grigorieff, N., *Proc. Nat'l. Acad. Sci.* **2015,** *112*, 11858-11863.
(40) Schütz, A. K.; Vagt, T.; Huber, M.; Ovchinnikova, O. Y.; Cadalbert, R.; Wall, J.; Güntert, P.; Böckmann, A.; Glockshuber, R.; Meier, B. H., *Angewandte Chemie International Edition* **2015,** *54*, 331-335.
(41) Xiao, Y.; Ma, B.; McElheny, D.; Parthasarathy, S.; Long, F.; Hoshi, M.; Nussinov, R.; Ishii, Y., *Nature Structural & Molecular Biology* **2015,** *22*, 499-505.
(42) Colvin, M. T.; Silvers, R.; Ni, Q. Z.; Can, T. V.; Sergeyev, I.; Rosay, M.; Donovan, K. J.; Michael, B.; Wall, J.; Linse, S.; Griffin, R. G., *J. Am. Chem. Soc.* **2016**, *138*, 9663-9674
(43) Elkins, M. R.; Wang, T.; Nick, M.; Jo, H.; Lemmin, T.; Prusiner, S. B.; DeGrado, W. F.; Stöhr, J.; Hong, M., *J. Am. Chem. Soc.* **2016,** *138*, 9840-9852.
(44) Ravotti, F.; Wälti, M. A.; Güntert, P.; Riek, R.; Böckmann, A.; Meier, B. H., *Biomolecular NMR Assignments* **2016,** *10*, 269-276.
(45) Wälti, M. A.; Ravotti, F.; Arai, H.; Glabe, C. G.; Wall, J. S.; Böckmann, A.; Güntert, P.; Meier, B. H.; Riek, R., *Proc. Nat'l Acad. Sci.* **2016,** *113*, E4976-E4984.
(46) Qiang, W.; Yau, W.-M.; Lu, J.-X.; Collinge, J.; Tycko, R., *Nature* **2017,** *541*, 217-221.
(47) Jaroniec, C. P.; Filip, C.; Griffin, R. G., *J. Am. Chem. Soc.* **2002,** *124*, 10728-10742.
(48) Hediger, S.; Meier, B. H.; Kurur, N. D.; Bodenhausen, G.; Ernst, R. R., *Chem Phys Lett* **1994,** *223*, 283-288.
(49) Wu, C. H.; De Angelis, A. A.; Opella, S. J., *J. Magn. Reson***2014,** *246*, 1-3.
(50) Lewandowski, J. R.; De Paëpe, G.; Eddy, M. T.; Struppe, J.; Maas, W.; Griffin, R. G., *J. Phys. Chem. B* **2009,** *113*, 9062-9069.
(51) Bennett, A. E.; Rienstra, C. M.; Auger, M.; Lakshmi, K. V.; Griffin, R. G., *J. Chem. Phys.* **1995,** *103*, 6951-6958.
(52) Goddard, T. D.; Kneller, D. G., SPARKY 3.115, University of California, San Francisco. 2008.
(53) Pines, A.; Gibby, M. G.; Waugh, J. S., *J. Chem. Phys.* **1973,** *59*, 569-590.

TOC GRAPHIC

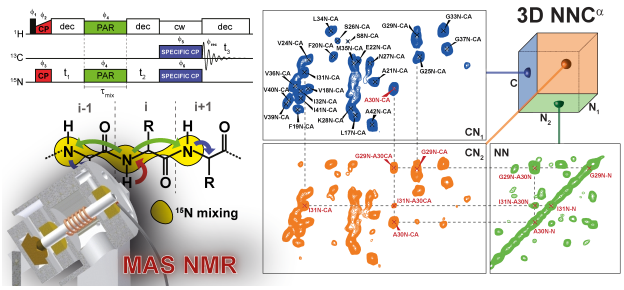
dec
PAR
dec
cw
dec
SPECIFIC CP
CP
PAR
SPECIFIC CP
i-1
i
i+1
^{15}N mixing
MAS NMR
3D NNC$^{\alpha}$
C
N_2
N_1
CN_1
CN_2
NN